Relationship between the mechanisms of gamma rhythm generation and the magnitude of the macroscopic phase response function in a population of excitatory and inhibitory modified quadratic integrate-and-fire neurons

Akihiko Akao,[1,*] Yutaro Ogawa,[2] Yasuhiko Jimbo,[1] G. Bard Ermentrout,[3] and Kiyoshi Kotani[2,4]
[1]*Graduate School of Engineering, The University of Tokyo, 7-3-1 Hongo, Bunkyo-ku, Tokyo 113-0033, Japan*
[2]*Research Center for Advanced Science and Technology, The University of Tokyo, 4-6-1 Komaba, Meguro-ku, Tokyo 153-8904, Japan*
[3]*Department of Mathematics, University of Pittsburgh, Pittsburgh, Pennsylvania 15260, USA*
[4]*JST, PRESTO, 4-1-8 Honcho, Kawaguchi-shi, Saitama 332-0012, Japan*

(Received 2 May 2017; revised manuscript received 6 November 2017; published 16 January 2018)

Gamma oscillations are thought to play an important role in brain function. Interneuron gamma (ING) and pyramidal interneuron gamma (PING) mechanisms have been proposed as generation mechanisms for these oscillations. However, the relation between the generation mechanisms and the dynamical properties of the gamma oscillation are still unclear. Among the dynamical properties of the gamma oscillation, the phase response function (PRF) is important because it encodes the response of the oscillation to inputs. Recently, the PRF for an inhibitory population of modified theta neurons that generate an ING rhythm was computed by the adjoint method applied to the associated Fokker-Planck equation (FPE) for the model. The modified theta model incorporates conductance-based synapses as well as the voltage and current dynamics. Here, we extended this previous work by creating an excitatory-inhibitory (E-I) network using the modified theta model and described the population dynamics with the corresponding FPE. We conducted a bifurcation analysis of the FPE to find parameter regions which generate gamma oscillations. In order to label the oscillatory parameter regions by their generation mechanisms, we defined ING- and PING-type gamma oscillation in a mathematically plausible way based on the driver of the inhibitory population. We labeled the oscillatory parameter regions by these generation mechanisms and derived PRFs via the adjoint method on the FPE in order to investigate the differences in the responses of each type of oscillation to inputs. PRFs for PING and ING mechanisms are derived and compared. We found the amplitude of the PRF for the excitatory population is larger in the PING case than in the ING case. Finally, the E-I population of the modified theta neuron enabled us to analyze the PRFs of PING-type gamma oscillation and the entrainment ability of E and I populations. We found a parameter region in which PRFs of E and I are both purely positive in the case of PING oscillations. The different entrainment abilities of E and I stimulation as governed by the respective PRFs was compared to direct simulations of finite populations of model neurons. We find that it is easier to entrain the gamma rhythm by stimulating the inhibitory population than by stimulating the excitatory population as has been found experimentally.

DOI: 10.1103/PhysRevE.97.012209

I. INTRODUCTION

Gamma oscillation, which is defined as collective rhythm in the brain of around 30–90 Hz, is thought to play an important role in brain function [1–4]. Therefore, understanding the generation mechanisms and dynamical properties of the gamma oscillation is important since this can inform us of pathologies in the rhythms, and how the collective oscillations respond to stimuli.

The mechanisms of gamma oscillation have been investigated experimentally [5–8]. A significant role for GABA (gamma-aminobutyric acid)-ergic inhibitory interneurons is suggested by many studies [6,7]. Such interneuron-loop-based gamma oscillation is called interneuron gamma (ING). On the other hand, gamma oscillations can emerge from the interaction between excitatory and inhibitory (E-I) populations. Such E-I interaction-based gamma oscillation is called pyramidal interneuron gamma (PING) [5,8].

The phase response function (PRF) characterizes how oscillations are shifted or reset due to external stimuli and form a nonparametric way to summarize the dynamical properties of gamma oscillations. For example, [9] derived the PRF for hippocampal gamma oscillations and used a simple firing rate model to explain the shape of the PRF. However, the relation between the generation mechanism of gamma and the phase response function is yet to be revealed.

To analyze the properties of gamma oscillations, a mathematical approach is useful [10,11]. Firing rate models are popular for describing population dynamics of neurons. This type of model arises as the mean field of a population of neurons, but the underlying dynamics is generally supposed to be asynchronous or the synapses sufficiently slow, something that is not the case for high-frequency oscillations [3,12,13]. The Fokker-Planck equation (FPE) allows one to analyze the population dynamics of noisy neuronal populations independent of synaptic time scales or the frequencies of oscillations

*Corresponding author. akao@neuron.t.u-tokyo.ac.jp

[14,15] where the relation between frequency and synaptic interactions has been investigated. However, these papers did not consider the behavior of such networks when stimulated, which requires the computation of the PRF. Recently, to solve these problems, we used the modified theta model to generate an ING-type network [16]. This model describes the voltage-dependent dynamics of theta neurons connected with chemical synapses, and its macroscopic dynamics can be analyzed using corresponding FPE. With this method, we were also able to compute the PRF. However, in that paper, we restricted our analysis to a purely inhibitory network.

In this study, we investigate the relation between the generation mechanism and dynamical properties (specifically the PRF) of the gamma oscillations. We develop a mathematical model for an E-I neuronal population using the modified theta model. We classify gamma oscillations by their generation mechanisms using bifurcation analysis on the FPE. We derive phase response functions which depend on the intrinsic nature of the oscillation and investigate how the PRFs differ depending on the generation mechanisms. We also show that there are some parameters in the Hopf bifurcation region where the PRF is positive for all the phases. Motivated by recent optogenetic experiments, we then use the PRFs in order to study the ranges of entrainment to pulsatile stimuli to either the excitatory or inhibitory populations.

II. METHODS

A. Population of excitatory and inhibitory neurons

The model of neuronal population in this study is based on the modified theta model, which arises when the quadratic integrate-and-fire model incorporates conductance-based synapses [16]. In this previous study, only the inhibitory neuronal population was considered [16]. Here, we broaden the coverage of the modified theta model to include E-I populations.

We consider a relatively small neuronal population [17] composed of 400 excitatory (E) and 100 inhibitory (I) neurons ($N_{\mathrm{E}} = 400$, $N_I = 100$). Excitatory neurons are considered as α-amino-3-hydroxy-5-methyl-4-isoxazolepropionic acid (AMPA) -ergic pyramidal cells. Inhibitory neurons are GABA-ergic interneurons.

The dynamics of membrane potential of the ith neuron in the X population, $V_X^{(i)}$, satisfies

$$C\frac{dV_X^{(i)}(t)}{dt} = -g_{LX}\frac{\left[V_X^{(i)}(t)-V_R\right]\left[V_X^{(i)}(t)-V_T\right]}{V_T-V_R} + I_X + \sigma_X\xi_X^{(i)} - \sum_{j=1}^{N_E} g_{E(j)}^{X(i)}\left[V_X^{(i)}(t)-V_E\right] - \sum_{j=1}^{N_I} g_{I(j)}^{X(i)}\left[V_X^{(i)}(t)-V_I\right], \quad (1)$$

where the membrane capacitance $C = 1\,[\mu\mathrm{F\,cm^{-2}}]$, firing threshold $V_T = -55\,[\mathrm{mV}]$, resting potential $V_R = -62\,[\mathrm{mV}]$, the Wiener process $\xi_X^{(i)}(t)$ satisfies $\langle\xi_X^{(i)}(t)\rangle = 0$, and $\langle\xi_X^{(i)}(t),\xi_X^{(i)}(t')\rangle = \delta_{ij}\delta(t-t')$. $\sigma = 1\,[\mu\mathrm{A\,ms^{1/2}\,cm^{-2}}]$ stands for the magnitude of the Wiener process. These equations and parameters come from our previous paper [16]. For the E-I population in this study, the leak conductance is set as $g_{\mathrm{LE}} = 0.08\,[\mathrm{mS\,cm^{-2}}]$ and $g_{\mathrm{LI}} = 0.1\,[\mathrm{mS\,cm^{-2}}]$ and the synaptic reversal potentials are set as $V_{\mathrm{E}} = 0\,[\mathrm{mV}]$ and $V_{\mathrm{I}} = -70\,[\mathrm{mV}]$. When I_{E} and I_{I} are not chosen as bifurcation parameters, the nominal value of the constant input current is set as $I_{\mathrm{E}} = I_{\mathrm{I}} = 1\,[\mu\mathrm{A\,cm^{-2}}]$ in this study. $g_{\mathrm{E}(j)}^{X(i)}$ and $g_{\mathrm{I}(k)}^{X(i)}$ are the conductance from excitatory jth and inhibitory kth neurons that are connected to ith neuron of the X population.

Following our previous study [16], we introduce a map from $V_X^{(i)}$ to $\theta_X^{(i)}$ as

$$V_X^{(i)} = \frac{V_R+V_T}{2} + \frac{V_T-V_R}{2}\tan\frac{\theta_X^{(i)}}{2}. \quad (2)$$

In this case, $V(t)$ will satisfy a quadratic integrate-and-fire equation with conductance-based synapses and a spiking threshold at $+\infty$ ($\theta = \pi$) and reset at $-\infty$ ($\theta = -\pi$) (see [16] for a complete derivation). Then the dynamics of $\theta_X^{(i)}$ is

$$\begin{aligned} C\frac{d\theta_X^{(i)}(t)}{dt} &= -g_{LX}\cos\theta_X^{(i)}(t) + \frac{2}{V_T-V_R}\left[1+\cos\theta_X^{(i)}(t)\right]\left[I_X+\sigma\xi_X^{(i)}(t)\right] \\ &\quad + \sum_{j=1}^{N_E} g_{E(j)}^{X(i)}\left\{\frac{2V_E-V_R-V_T}{V_T-V_R}\left[1+\cos\theta_X^{(i)}(t)\right] - \sin\theta_X^{(i)}(t)\right\} \\ &\quad + \sum_{k=1}^{N_I} g_{I(k)}^{X(i)}\left\{\frac{2V_I-V_R-V_T}{V_T-V_R}\left[1+\cos\theta_X^{(i)}(t)\right] - \sin\theta_X^{(i)}(t)\right\}. \end{aligned} \quad (3)$$

The dynamics of $g_{Y(j)}^{X(i)}$, which represents the synaptic conductance from the jth neuron of type Y to the ith neuron of type X, is described by a second-order ordinary differential equation as

$$\tau_{r(XY)}\tau_{d(XY)}\frac{d^2g_{Y(j)}^{X(i)}(t)}{dt^2} + (\tau_{r(XY)}+\tau_{d(XY)})\frac{dg_{Y(j)}^{X(i)}(t)}{dt} + g_{Y(j)}^{X(i)}(t) = \overline{g}_Y^X\sum_j\delta(t-t^{(j)}), \quad (4)$$

where $\tau_{r(XY)}$ represents the rise time of the synaptic conductance from type Y to type X neuron, $\tau_{d(XY)}$ represents the decay time, and $t^{(j)}$ is a firing time of presynaptic neuron j. $\overline{g}_X^Y$ is a parameter to determine the peak conductance. The

TABLE I. Parameters for synaptic conductance in Eq. (4).

	$\tau_{r(X,Y)}$ (ms)	$\tau_{d(X,Y)}$ (ms)	$\bar{g}_Y^X$ (mS/cm^2)
$g_{\mathrm{E}}^{\mathrm{E}}(t)$: AMPA on pyramidal cell	0.5	2	0.013
$g_{\mathrm{E}}^{\mathrm{I}}(t)$: AMPA on interneuron	0.5	2	0.010
$g_{\mathrm{I}}^{Ea}(t)$: GABA on pyramidal cell	0.5	5	0.173
$g_{\mathrm{I}}^{\mathrm{I}}(t)$: GABA on interneuron	0.5	5	0.138

effect of the synaptic interaction depends on, not only the kind of neurotransmitter released from the presynaptic neuron, but also the kind of postsynaptic neuron which receives the neurotransmitter. So we have to consider $2 \times 2 = 4$ kinds of $g_Y^X(t)$. Y represents the emitted neurotransmitter from presynaptic cell: E or I. X represents the postsynaptic cell type: E or I. We set the area of neuron as 2.9×10^{-4} cm^2 [18], so the units of the equation are consistent with the previous study [13]. $\bar{g}_X^Y$ is chosen as to match the physiological plausible values [13,19,20]. The parameters for four kinds of $g_Y^X(t)$ are listed in Table I.

Here we consider a situation in which all the synapses are randomly connected from Y type to X type with a probability of p_{XY}. With such couplings, the corresponding FPE of the neuronal population would be a set of $N_{\mathrm{I}} + N_{\mathrm{E}}$ FPEs where each FPE describes each individual neuronal dynamics. In order to reduce the number of FPEs, here we introduce a strong assumption to treat each neuron homogeneously. Under the condition that the synaptic couplings have probabilities p_{YX}, we adopt a mean-field approximation which homogenizes all the conductance variables into mean-field conductance [13]. After adopting this approximation, Eq. (4) reads as

$$\tau_{r(XY)}\tau_{d(XY)}\frac{d^2 g_Y^X(t)}{dt^2} + (\tau_{r(XY)} + \tau_{d(XY)})\frac{dg_Y^X(t)}{dt} + g_Y^X(t) = \bar{g}_Y^X(t) p_{XY} N_Y A_Y(t), \tag{5}$$

where N_Y is a number of type Y neurons and A_Y is the firing probability of type Y neurons. p_{XY} are variable parameters in this study in order to unveil how the modulation of synaptic strength contributes to the behavior of the macroscopic oscillation.

Now the whole dynamics of randomly connected E-I population is described as the combination of Eq. (3) for E,I and Eq. (5) for the four types of interactions.

B. Fokker-Planck equation of the E-I population

The FPE [21,22] of the modified theta model is relatively easy to analyze because of its periodic boundary condition. The corresponding FPE for Eq. (1) can be derived as in [16]:

$$\frac{\partial P_X(\theta,t)}{\partial t} = -\frac{\partial}{\partial\theta}\left(\frac{1}{C}\left\{-g_{LX}\cos\theta + c_1(1+\cos\theta)\left(I_X - \frac{c_1\sigma^2}{2C}\sin\theta\right) + \sum_Y g_Y^X(t)[c_{2Y}(1+\cos\theta) - \sin\theta]\right\}P_X(\theta,t)\right) + \frac{c_1^2\sigma^2}{2C^2}\frac{\partial^2}{\partial\theta^2}[(1+\cos\theta)^2 P_X(\theta,t)], \tag{6}$$

where $c_1 = 2/(V_T - V_R)$, $c_{2Y} = (2V_Y - V_R - V_T)/(V_T - V_R)$.

By introducing $G_Y^X = (g_{1Y}^X, g_{2Y}^X)^T = (g_Y^X, dg_Y^X/dt)^T$, the dynamics of synaptic conductance can be written as

$$\frac{dG_Y^X}{dt} = \begin{bmatrix} 0 & 1 \\ c_{3(XY)} & c_{4(XY)} \end{bmatrix} G_Y^X + \begin{bmatrix} 0 \\ \frac{c_{5(XY)} g_{LY}}{C} P_Y(\pi,t) \end{bmatrix}, \tag{7}$$

where $c_{3(XY)} = -1/(\tau_{r(XY)}\tau_{d(XY)})$, $c_{4(XY)} = -(\tau_{r(XY)} + \tau_{d(XY)})/(\tau_{r(XY)}\tau_{d(XY)})$, and $c_{5(XY)} = \bar{g}_Y^X p_Y^X N_Y/(\tau_{r(XY)}\tau_{d(XY)})$. Note that, in this FPE, the flux at $\theta = \pi$ in the Y population is given by $g_{LY} P_Y(\pi,t)/C$ [23,24].

Now the whole dynamics of the E-I population is described by two PDEs [Eq. (6)] that represent the dynamics of membrane potential $V_X^{(i)}$ (via the transformed coordinates, $\theta_X^{(i)}$) for all the neurons in the population and synaptic conductance dynamics g_Y^X.

In this paper, numerical integration of these equations was conducted with $dt = 0.005$. PDEs are integrated by the Crank-Nicholson method with discretization of $\theta \in [0,2\pi)$ into $n_x = 200$ bins.

C. Bifurcation analysis and classification of gamma oscillation based on generation mechanism

In order to investigate how the change of synaptic strength p_Y^X and external input to the population I_X modulates the emergence of gamma oscillation, we conducted a bifurcation analysis on the FPEs and chose p_Y^X and I_X as bifurcation parameters. Bifurcation analyses on the FPEs are conducted using XPPAUT [25] with discretization into only $n_x = 90$ bins for the purpose of computational efficiency.

In previous research on the gamma oscillation, two types of generation mechanisms are proposed: ING and PING. These two mechanisms are characterized by "What is the driver of I population." In the case of ING, the driver for the I population is an excitatory current without any rhythmicity, which corresponds to I_{I} in our model. On the other hand, in the case of PING, the driver for the I population is the excitatory rhythmic current from the excitatory population, which is represented by p_{IE} in our model [26]. So, in our model, we called oscillatory parameters with $I_{\mathrm{I}} > 0$ and $p_{\mathrm{IE}} = 0$ ING, because only the excitatory current without rhythmicity

(I_I) is driving I cells. Also, we named oscillatory parameters where $I_I = 0$ and $p_{IE} > 0$ as PING, because only the rhythmic excitatory current from E cells is driving I cells.

D. Phase reduction of Fokker-Planck equation

The adjoint method is an analytic method to derive the phase response function of a limit cycle oscillator [12,27]. If there is a limit cycle solution to some dynamical system, we linearize the dynamics in the vicinity of the limit cycle orbit and compute the unique (up to scaling) periodic solution to the adjoint linear operator arising from the linearization. Recently, the adjoint method was extended to macroscopic collective rhythms [16,28]. Following these studies, we can derive the macroscopic phase response function using an adjoint method in the E-I population.

We define the limit cycle orbit as $P_{0X}(\theta,t)$ and $G^Y_{0X}(t) = (g^X_{0Y}, dg^X_{0Y}/dt)^T$. These are periodic functions defined in $0 \leqslant t < T_{\rm macro}$, where $T_{\rm macro}$ is the period of the macroscopic gamma oscillation. The zero phase is defined as the peak timing of the inhibitory neuronal firing rate. The dynamics P_X and G^Y_X can be decomposed into $P_X(\theta,t) = P_{0X}(\theta,t) + Q_X(\theta,t)$ and $G^X_Y(\theta,t) = G^X_{0Y}(\theta,t) + H^X_Y(\theta,t)$ where $H^X_Y = (h^X_{1Y}, h^X_{2Y})^T$. The linearized equation $Q_X(\theta,t)$ and $H^X_Y(\theta,t)$ can be written as

$$\frac{\partial Q_X}{\partial t} = -\frac{\partial}{\partial\theta}\left(\frac{1}{C}\left\{-g_{LX}\cos\theta + c_1(1+\cos\theta)\left(I_X - \frac{c_1\sigma}{2C}\sin\theta\right) + \sum_Y g^X_{0Y}[c_{2Y}(1+\cos\theta) - \sin\theta]\right\}Q_X\right)$$
$$-\sum_Y \frac{\partial}{\partial\theta}\left\{\frac{1}{C}[c_{2Y}(1+\cos\theta) - \sin\theta]P_0(t)\right\}h^X_{1Y} + \frac{c_1^2\sigma^2}{2C^2}\frac{\partial^2}{\partial\theta^2}[(1+\cos\theta)^2 Q_X] \tag{8}$$

and

$$\frac{dH^X_Y}{dt} = \begin{bmatrix} 0 & 1 \\ c_{3(XY)} & c_{4(XY)} \end{bmatrix} H^X_Y + \begin{bmatrix} 0 \\ \frac{c_{5(XY)}g_{LY}}{C} Q_Y(\pi,t) \end{bmatrix}. \tag{9}$$

Then, the adjoint equation for this ODE-PDE system is

$$\frac{\partial Q^*_X}{\partial t} = -\frac{1}{C}\left[-g_{XL}\cos\theta + c_1(1+\cos\theta)\left(I_X - \frac{c_1\sigma^2}{2C}\sin\theta\right) + \sum_Y g^X_{Y0}[c_{2Y}(1+\cos\theta) - \sin\theta]\right]\frac{\partial}{\partial\theta}Q^*_X(\theta,t)$$
$$-\sum_Y \delta(\theta-\pi)\frac{g_{YL}c_{5(XY)}}{C}h^{X*}_{2Y} - \sum_Y \frac{c_1^2\sigma^2}{2C^2}(1+\cos\theta)^2\frac{\partial^2}{\partial\theta^2}Q^*(\theta,t), \tag{10}$$

$$\frac{dH^{X*}_Y}{dt} = -H^{X*}_Y\begin{bmatrix} 0 & 1 \\ c_{3(XY)} & c_{4(XY)} \end{bmatrix} + \left[\int_0^{2\pi}\frac{\partial}{\partial\theta}\left\{\frac{1}{C}[c_{2Y}(1+\cos\theta) - \sin\theta]P_{0X}(t)\right\}Q^*_X d\theta \quad 0\right]. \tag{11}$$

To derive zero the eigenfunction (corresponding to the null space) of Eqs. (10) and (11), we numerically integrate Eqs. (10) and (11) backwards in time [29]. The numerical integration was conducted by the Lax-Wandroff and Crank-Nicholson method with $dt = 0.005$ and $n_x = 200$.

The normalizing condition for the zero eigenfunction is

$$\sum_X\left[\int_0^{2\pi}\left(Q^*_X\frac{\partial P_{0X}}{\partial t}\right)d\theta\right] + \sum_X\sum_Y H^{X*}_{0Y}\frac{dG^X_{0Y}}{dt}$$
$$= \omega = \frac{2\pi}{T_{\rm macro}}. \tag{12}$$

Finally, the macroscopic phase sensitivity is derived as

$$Z_X(\Theta) = \int_0^{2\pi}\frac{c_1(1+\cos\theta)}{C}P_{0X}(\theta,\Theta)\frac{\partial}{\partial\theta}Q^*_{0X}(\theta,\Theta)d\theta. \tag{13}$$

The macroscopic phase sensitivity measures how the macroscopic phase shifts in reaction to the external perturbations applied to all of the neurons in the X population. We now can examine how the macroscopic phase sensitivity transforms as the synaptic strength or other physiological parameters change.

III. RESULT

A. Verification of the correspondence between the neuronal population model and Fokker-Planck equation

To confirm that the FPEs are valid to elucidate the population dynamics of neuronal models, we demonstrated that the results of numerical simulation of the FPEs, Eqs. (7) and (8), are similar to those for the finite population of neurons, Eqs. (4) and (6). In Figs. 1(a)–1(f), $p_{II} = p_{IE} = p_{EI} = p_{EE} = 0.1$ are chosen as representative parameters for the steady state, while in Figs. 1(g)–1(l), $p_{EI} = p_{EE} = 0.1$, $p_{II} = 0.2$, and $p_{IE} = 0.05$ are chosen for a typical oscillatory state.

Numerical simulations of the population of theta neurons are shown in Figs. 1(b)–1(d) and 1(h)–1(j). Numerical simulations of corresponding Fokker-Planck equations are shown in Figs. 1(e) and 1(k). Although there are fluctuations in the neuronal model due to their finite-size effect, we can see the consistency between the dynamics of the neuronal population and thecorresponding Fokker-Planck equation. In Figs. 1(f)

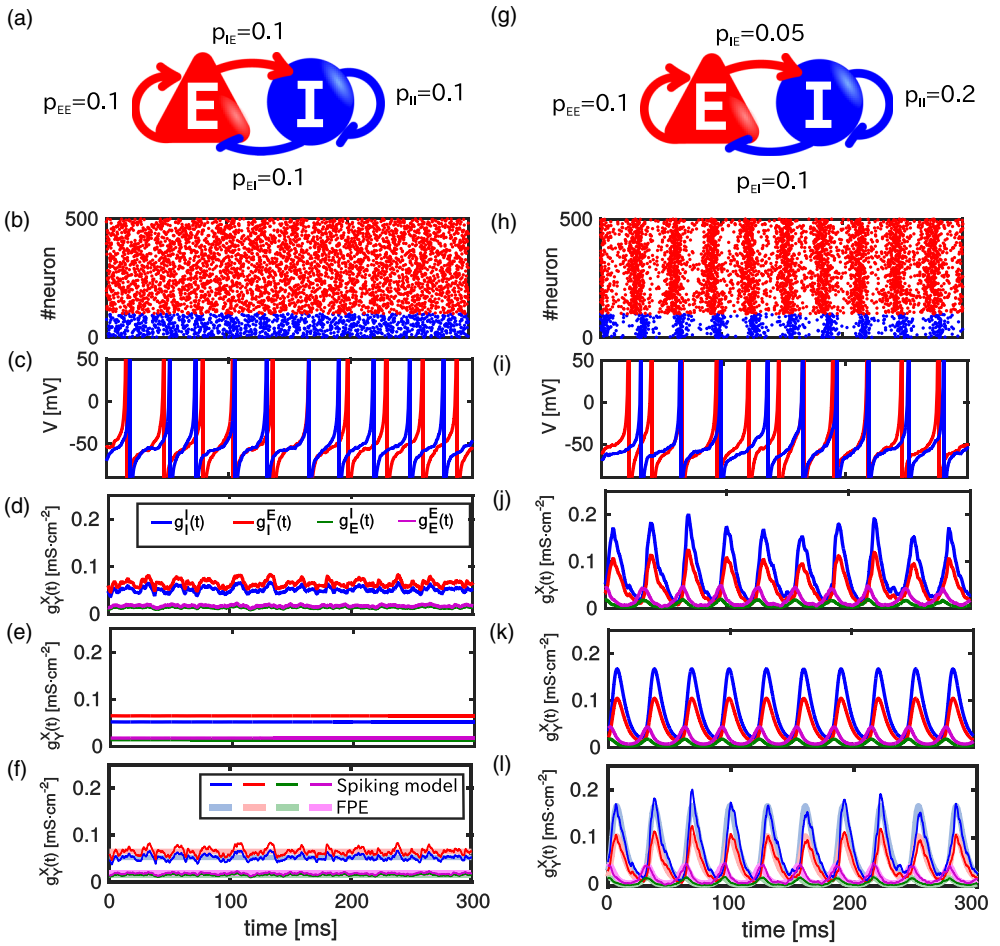

FIG. 1. Dynamics of E-I neuronal population simulated with both the full spiking neuronal model and corresponding Fokker-Planck equation. (a)–(f) Stable steady state. (g)–(l) Oscillatory state. (a),(g) Network diagram. (b),(h) Raster of the excitatory (red, light gray) and inhibitory (blue, dark gray) neurons. (c),(i) Membrane potential of representative neurons. (d),(j) Time series of synaptic conductance $g_Y^X(t)$ simulated with the spiking neuronal model. (e),(k) Conductances from the Fokker-Planck equation. (f),(l) Overlay of the two $g_Y^X(t)$: Spiking neuronal population and FPE. Note that the two simulated time series are in good agreement, which indicates the validity of the Fokker-Planck equation. Parameters were set as specified in the Methods section such as $I_{\mathrm{I}} = I_{\mathrm{E}} = 1$.

and 1(l), to compare the dynamics of the two models, we plotted the two simulated time series in one panel. The two sets of time series are in good agreement, which indicates the validity of the Fokker-Planck equation.

B. Bifurcation diagrams and classification of the gamma oscillation

We conducted a bifurcation analysis to investigate the influence of synaptic connection p_{YX} and external drive I_X on the emergence of the gamma oscillation. Figure 2(a), p_{II}, which represents the synaptic strength of local reccurent inhibition, and p_{IE}, which represents the synaptic strength from E cells to I cells, are chosen as bifurcation parameters. In Fig. 2(b), we chose I_{I} and p_{IE} as bifurcation parameters because these two parameters are directly related to the definition of ING and PING in our model [see method (c)].

As a result of the bifurcation analysis, oscillatory parameter regions via a Hopf bifurcation are found in both Figs. 2(a) and 2(b). Four representative parameter sets are chosen and marked in Figs. 2(a) and 2(b). In Fig. 2(a), for $p_{\mathrm{IE}} = 0$, oscillation emerges for large p_{II} (marked as a blue dot) and as p_{IE} increases, the curve of Hopf bifurcations moves downward until it crosses the $p_{\mathrm{II}} = 0$ line (marked as the orange dot). In Fig. 2(b), the same parameter as the blue dot in Fig. 2(a) is also marked as the same color (blue dot), which is also located close to the Hopf boundary. As p_{IE} increases, the Hopf boundary linearly moves downward and also crosses the $I_I = 0$ line (marked as a red dot). Note that in Fig. 2(b), the blue dot is ING-type oscillation because $p_{\mathrm{IE}} = 0$ means no excitatory current is injected from the E population for I cells and I cells are purely driven by the external current I_{I}. Also, the red dot in Fig. 2(b) is a PING-type oscillation because $I_I = 0$ means no external current exists for the I cells and so I cells are purely driven by the excitatory current from the E cells.

The time series for each of the representative parameter sets are shown in Figs. 2(c)–2(f). The frequency of the oscillation is around 40 Hz for all the parameters so that they are all in the gamma range.

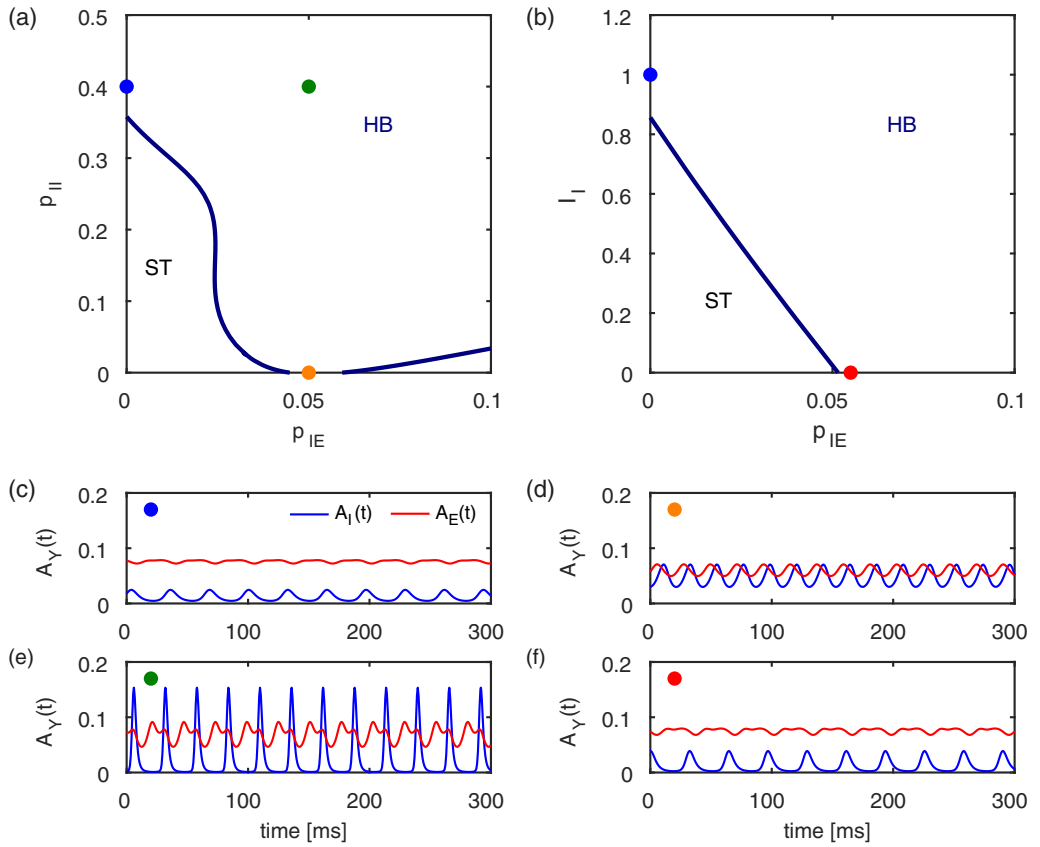

FIG. 2. (a),(b) Bifurcation diagrams of the FPE. ST and HB stand for steady state and Hopf bifurcation, respectively. (a) Bifurcation diagram with $(I_{\rm I}, p_{\rm EI}, p_{\rm EE}) = (1,0.1,0.2)$. Representative parameters of blue, orange, and green dots are chosen as $(p_{\rm IE}, p_{\rm II}) = (0,0.4)$, (0.05,0), and (0.05,0.4), respectively. (B) Bifurcation diagram with $(p_{\rm II}, p_{\rm EI}, p_{\rm EE}) = (0.4,0.1,0.2)$. Representative parameters of blue and red dots are chosen as $(p_{\rm IE}, I_{\rm I}) = (0,1)$ and (0.05,0), respectively. Note that the two blue dots in (a) and (b) correspond to the same parameter. (c)–(f) Time series of $A_Y(t)$ which represents the firing rate of the Y population simulated with representative parameters chosen in (a) and (b). (c) Blue. (d) Orange. (e) Green. (f) Red. Other parameters are set as specified in the Methods section such as $I_E = 1$.

C. Verification of macroscopic phase response function derived by the adjoint method

We computed the macroscopic PRF [or, more precisely, the adjoints, $Z_X(\phi)$] of each of the gamma types to investigate any differences. The PRF for each of the gamma types at the representative points is shown in Fig. 3. Here we define the phase ϕ of the oscillation to be scaled to $\phi \in [0,2\pi)$ with $\phi = 0$ corresponding to the peak of the inhibitory population rhythm. Thus, for a variable, $q(t)$, the value at phase ϕ is $q[T_{\rm macro}\phi/(2\pi)]$ where $T_{\rm macro}$ is the period of the oscillation. We computed these using the adjoint method (see Methods), and to confirm the validity of the PRFs derived by the adjoint method, the phase sensitivity is also computed by a perturbation method and compared. The phase sensitivity of the X population at phase ϕ is defined as $\Delta\phi/\Delta I_X$ where $\Delta\phi$ is a macroscopic phase shift caused by impulsive perturbation ΔI_X to I_X, the bias current to the entire population X, at phase ϕ. Representative parameters are chosen from Figs. 2(a) and 2(b). In each panel of Fig. 3, we see an excellent match between the adjoint and direct perturbation methods.

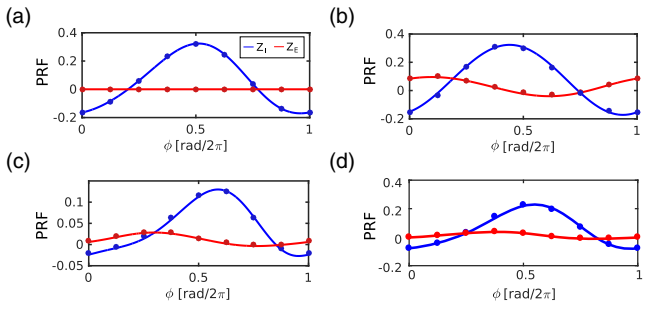

FIG. 3. Macroscopic PRFs of gamma oscillation: (a) Blue dot. (b) Orange dot. (c) Green dot. (d) Red dot. Blue and red represent $Z_{\rm I}$ and $Z_{\rm E}$, respectively. Solid line is computed by the adjoint method and dots are computed by the perturbation method.

In Fig. 3(b), both PRFs are generally sinusoidal. In Fig. 3(a), $Z_{\rm I}$ is also generally sinusoidal; however, Z_E is zero for all the phases. This is because the E population has no effect on the I population when the rhythm is generated (i.e., $p_{\rm IE} = 0$).

D. Comparison of phase response function between ING- and PING-type oscillation

To reveal how the change of synaptic strength p_{YX} and external current I_X affects the responses to stimuli, we investigate how the PRFs change as the type of the gamma oscillation changes.

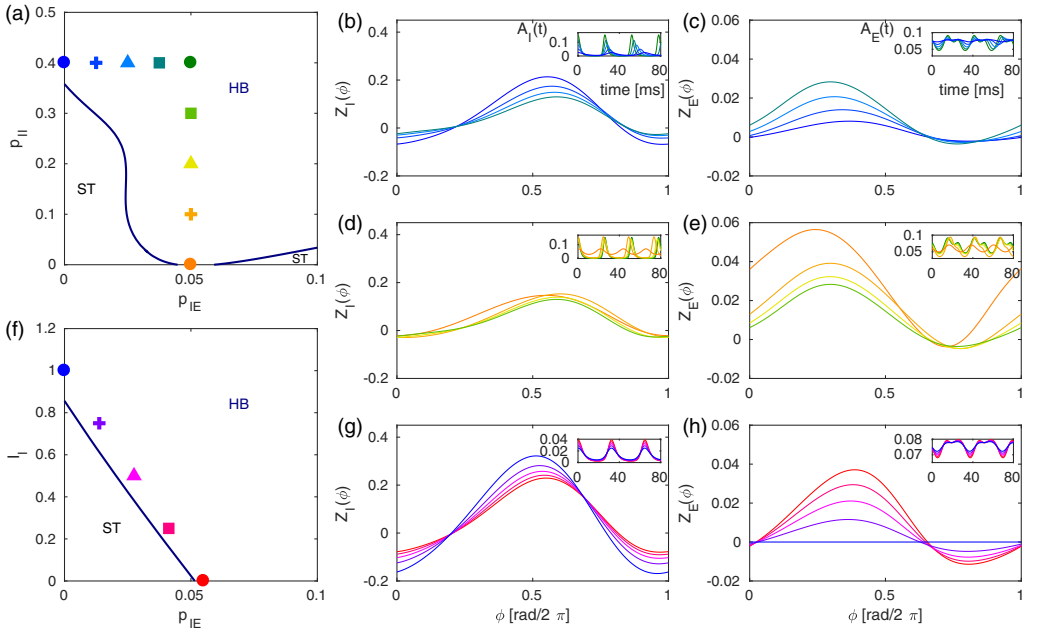

FIG. 4. Comparison of phase response function between different paramaters. (a) Parameter region of gamma oscillations and representative parameters. (b),(c) PRF transition from blue cross to green dot (left to right). (d),(e) PRF transition from orange cross to green dot (bottom to top). (F) Parameter region of gamma oscillations and representative parameters. Note that the blue and red dots correspond to ING and PING, respectively. (g),(h) PRF transition from ING (blue dot) to PING (red dot). (b),(d),(g) Main panel: Z_{I}. $A_{\mathrm{I}}(t)$ is plotted in the inset at top right. (c),(e),(h) Main panel: Z_{E}. $A_{\mathrm{E}}(t)$ is plotted in the inset at top right.

We derived PRFs by the adjoint method for representative parameters which were chosen with equally spaced intervals as shown in Figs. 4(a) and 4(f). In Fig. 4(a), the parameters are set so that p_{IE} (drive to I cells from E cells) and I_{I} (external drive to I cells) changes linearly from a green mark to blue and orange marks. We show the changes in the PRF at these points in Figs. 4(b)–4(e); also the time series of the firing rate of the populations $A(t)$ are shown in the inset. In Fig. 4(f), parameters are changed linearly from a blue mark to a red mark. The changes in the PRF at these points are shown in Figs. 4(g) and 4(h).

In panels (b) and (c), we see several changes as we increase p_{IE}: the size of Z_{I} shrinks and Z_{E} grows; in all cases, however, Z_{I} is larger in magnitude than Z_{E}; and the PRF is mostly positive for Z_{E}, but Z_{I} maintains some negative lobes near the 0 (and 2π) phase. In the other direction [Figs. 4(d) and 4(e)] as p_{II} decreases from the green dot, Z_{E} gets larger, while Z_{I} barely changes.

In panels (g) and (h), how the PRF changes from the blue dot to the red dot is shown. Note that the blue dot is an ING-type oscillation because I cells are driven by I_{I}. On the other hand, the red dot is a PING-type oscillation driven by p_{IE}. As the generation mechanism changes from ING to PING, the magnitude of Z_{I} shrinks, while Z_{E} grows. In addition, the frequency of the oscillation of $A_X(t)$, shown in the insets, is close to constant during the change from ING to PING. In the comparison between ING and PING, the magnitude of Z_{E} is most sensitive to the generation mechanism. In the case of ING, the amplitude of Z_{E} is zero because I cells are not excited by E cells and so perturbations of the E cells will not affect the I cells. The amplitude of Z_{E} grows as the parameter changes from ING to PING, reflecting the increasing involvement of excitation from E cells. As shown in panels (f)–(h), when the frequency of the oscillation and the amplitude of Z_{I} are similar, the amplitude of Z_{E} reflects the degree of attendance of E cells to rhythmogenesis of the gamma oscillation, which makes it easier to distinguish the generation mechanism of the gamma oscillation is ING-like or PING-like.

In addition, there are important consistent differences between the shapes of Z_{I} and Z_{E}. Most obvious is that Z_{E} is always smaller in magnitude than Z_{I} so that the network will be less sensitive to inputs to the E population than to those in the I population. Another interesting difference is that the skew of Z_{E} is toward the left, while that of Z_{I} is toward the right. In [30,31], the authors showed that PRFs that skew to the right are more conducive to synchronization.

E. A purely positive phase response function

In order to further investigate the properties of PING-type oscillations, we computed the PRF over several parameters. First, we conducted a bifurcation analysis for the PING-type oscillation with $p_{\mathrm{II}} = 0$. We fix the E-I coupling parameters as $(p_{\mathrm{IE}}, p_{\mathrm{EI}}) = (0.05, 0.1)$ and vary p_{EE} and I_{E} for the bifurcation parameters. The result of this analysis is shown in Fig. 5(a). Next, we computed PRFs along the marked points in Fig. 5(a), marked as a circle, cross, triangle, and square. In Figs. 5(b)–5(e), the PRFs for each parameter are shown. The excitatory PRF (Z_E) appears to always be non-negative, while the inhibitory PRF (Z_{I}) has both negative and positive lobes near the Hopf bifurcation as expected [32]. As we progress away from the bifurcation point, both PRFs become non-negative. They both become smaller in magnitude as well, but barely change once past the bifurcation point.

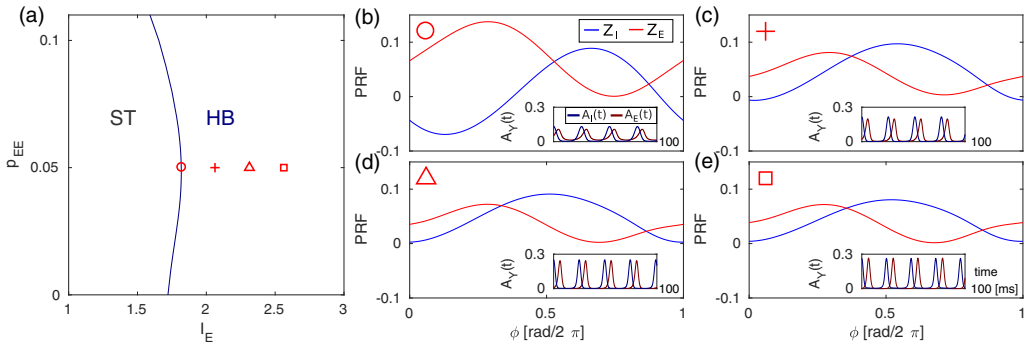

FIG. 5. A non-negative PRF. (a) Parameter region of the four and representative parameters. (b)–(e) PRF computed at the representative parameters. Red is Z_I. Blue is Z_E. (b) PRF at circle. (c) PRF at cross. (d) PRF at triangle. (e) PRF at square.

F. Entrainment of the pulsatile stimuli

According to a recent experimental study, the response of gamma oscillations to an external periodic stimulus varies depending on what kind of cell is being stimulated. For example, in the case of mouse cortex, when inhibitory cells are stimulated by a gamma-band periodic pulse train, the increase of power of gamma oscillation is larger than that for the excitatory case [33]. We claim that the origin of the cell-type-specific response comes from the difference of the entrainment ability to the pulsatile stimuli between I and E populations. To test our assertion, we evaluate the entrainment abilities of I and E populations through direct simulation of the spiking network and via weak coupling using our PRF.

We applied a periodic force $I_{\rm ext}(t)$, whose frequency is slightly different from the natural frequency of gamma oscillation, as

$$I_{\rm ext}(t) = I_{\rm app} R(t) \tag{14}$$

and

$$R(t) = \begin{cases} 1 & t \bmod \left(\frac{2\pi}{\omega_{\rm app}}\right) \leqslant t_{\rm app} \\ 0 & t \bmod \left(\frac{2\pi}{\omega_{\rm app}}\right) > t_{\rm app}, \end{cases} \tag{15}$$

where, $I_{\rm app}$, $\omega_{\rm app}$, and $t_{\rm app}$ represent the strength, frequency, and pulse length of each pulse train. $t_{\rm app}$ is set as 1 ms to imitate the light pulses used in [33]. $I_{\rm ext}$ is added to the bias currents, $I_{\rm I}, I_{\rm E}$ of either the inhibitory or excitatory cells to investigate the difference of the synchronization differences between the two populations. When $I_{\rm app}$ is applied to the X population whose natural frequency is $\omega_{\rm nat}$, the phase equation of macroscopic phase ϕ is written as

$$\dot{\phi} = \omega_{\rm nat} + Z_X(\phi) I_{\rm app}\left(\frac{\psi}{\omega_{\rm app}}\right), \tag{16}$$

where $\psi = (\omega_{\rm app} t \bmod 2\pi)$ is the phase of $I_{\rm app}$.

Introducing a new dynamical variable $\Phi = \phi - \psi$ which describes the phase difference between the macroscopic oscillation ϕ and external periodic force ψ, the dynamics of Φ is described as

$$\dot{\Phi} = (\omega_{\rm nat} - \omega_{\rm app}) + \Gamma_X(\Phi), \tag{17}$$

where $\Gamma_X(\Phi) = \frac{1}{2\pi}\int_0^{2\pi} Z_X(\Phi+\psi) I_{\rm app}(\psi/\omega_{\rm app}) d\psi$ is called phase coupling function [27]. $\dot{\Phi} = 0$ is achieved when the frequency difference $\Delta\omega_{\rm in} = \omega_{\rm app} - \omega_{\rm nat}$ satisfies $\min[\Gamma_X(\Phi)] \leqslant \Delta\omega_{\rm in} \leqslant \max[\Gamma_X(\Phi)]$, which means phase locking between ϕ and ψ.

To validate the prediction of the phase reduction theory, we computed the locking region by direct simulation of the spiking population. The frequency of the simulated gamma oscillation is evaluated by the mean frequency for the simulated time span. The simulated time span is 2×10^4 (ms) for Fig. 6.

We chose two representative parameters. One is $(p_{\rm IE}, p_{\rm II}) = (0.0375, 0.4)$ [green square in Fig. 4(a)], which is close to ING. The other is $(p_{\rm IE}, I_{\rm I}) = (0.07, 0)$ in Fig. 4(f), which is a PING-type oscillation. We computed the coupling region for the external periodic pulse train. In Fig. 6, the locking region predicted from the phase response function is shown as black triangles, while the result of simulation of periodic forcing in spiking population is shown by the surface plot. The locking region predicted by the phase reduction and direct simulations are similar in Fig. 6. The consistency indicates the phase reduction theory on macroscopic gamma oscillation correctly predicts the results of direct simulations of the spiking population. We also note the computation of the locking region was much faster by the phase reduction theory than by the direct simulations. This indicates the macroscopic phase reduction of gamma oscillation provides an efficient way to analyze synchronization phenomena of gamma oscillations. In addition, comparing Figs. 6(a) and 6(b), the locking region of the inhibitory population is wider than that of the excitatory population. This indicates that the I population has a higher entrainment ability to gamma-band pulsatile stimuli than the E population. Moreover, comparing (c) and (c), (d) has a wider locking region than (c), which suggests that the E cells in the PING oscillation has a higher entrainment ability than that in ING-flavored gamma oscillations.

IV. DISCUSSION

We extended the modified theta model [16] to coupled excitatory and inhibitory populations in order to describe the dynamics of the emergent gamma oscillations. There are several kinds of mathematical models capable of describing the population dynamics of neurons. Firing rate models, such as the Wilson-Cowan model are widely used to describe such systems. Although firing rate models are popular and simple to implement, it is hard to connect them to fast oscillatory activity such as gamma oscillations because the time constant

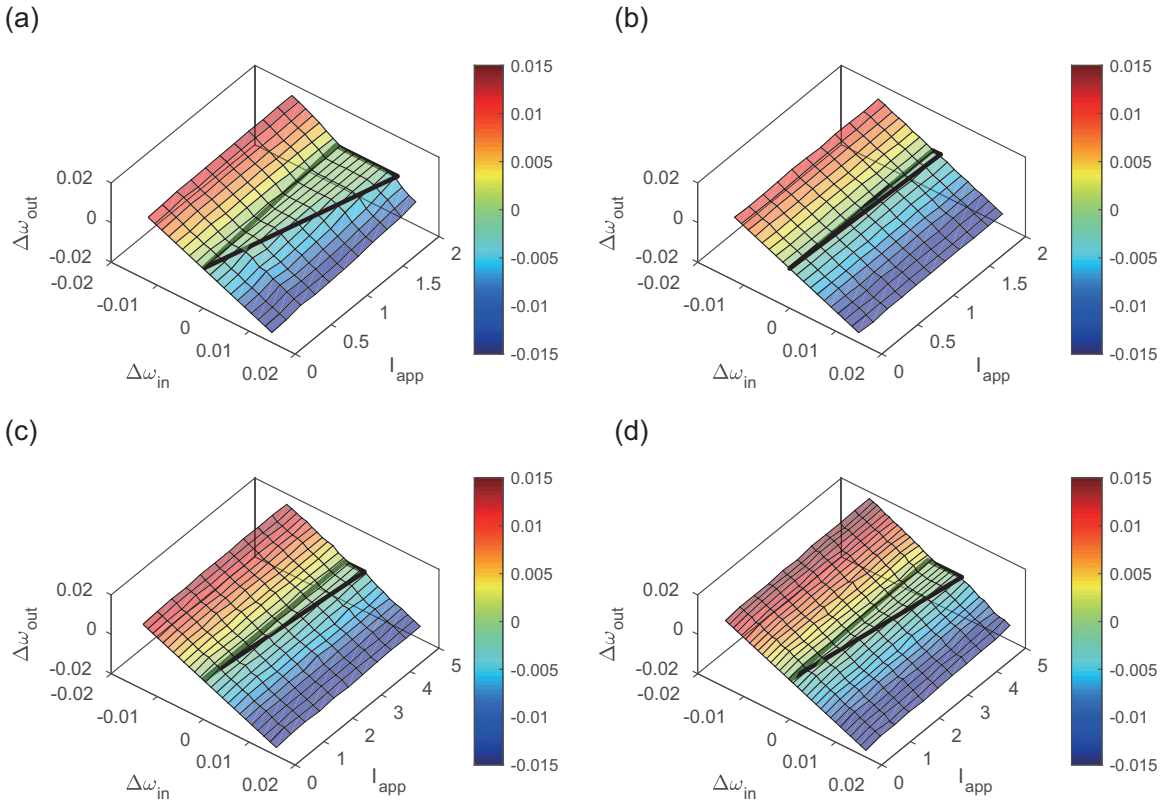

FIG. 6. Locking regions of the gamma oscillations under external pulsatile stimuli. $\Delta\omega_{out} = \omega_{forced} - \omega_{app}$ represents the difference between the observed frequency (ω_{forced}) and the applied frequency (ω_{app}). When $\Delta\omega_{out}$ is close to zero, that means the gamma oscillation is locking to the pulsatile stimulus. I_{app} represents the strength of pulsatile stimulus. $\Delta\omega_{in} = \omega_{app} - \omega_{nat}$ represents the difference between the frequency of the applied pulsatile stimulus ω_{app} and the natural (unforced) frequency of the gamma oscillation ω_{nat}. The surface plot shows the result of direct simulation of the spiking population and the black triangle represents locking regions derived from the phase reduction method. (a)–(c) Entrainment ability of gamma oscillation whose parameters are taken from the green square in Fig. 4(a). (a) Pulsatile stimuli applied to the inhibitory population. (b) Pulsatile stimuli applied to the excitatory population. (c) Enlarged view of (b). (d) Entrainment ability of gamma oscillation whose parameters are taken from PING-type oscillation [$I_I = 0$, $p_{IE} = 0.07$ in Fig. 4(f)]. Note that the phase reduction theory (black triangle) successfully predicts the locking regions which is confirmed by the direct simulations of the spiking population (surface plot). Also, note that the inhibitory population has a larger locking region than that of the excitatory population. In panel (d), the locking region is wider than that in panel (c).

of the firing rate model restricts the upper limit of the frequency which can be reproduced in the model [12]. In this research, we use a Fokker-Planck equation to describe and analyze the fast neural oscillations. Figure 1 shows that the FPE describes the macroscopic oscillations from spiking models of neurons quite well. While individual neurons spike irregularly, the macroscopic rhythm is quite robust and regular, as shown experimentally [34].

In this paper, we introduced variability through external noise much as earlier work by Brunel *et al.* have done in the leaky integrate-and-fire model [13]. Recently, Refs. [14,35,36] have explored the macroscopic dynamics of spiking networks of neurons that have *quenched* variability; that is, rather than external noise as in the present paper, they have introduced randomness in the parameters, mainly the applied currents to the neurons. By using the quadratic integrate and fire (or, equivalently, the theta neuron), they are able to use the Ott-Antonsen ansatz [37] to reduce the FPE to a low-dimensional dynamical system as long as the random parameters are taken from a Lorentzian distribution. For example, with instantaneous synaptic connections, an EI network becomes a simple four-dimensional dynamical system that produces PING-type oscillations.

Reference [36] used this method to compute the phase response functions of such an EI network and compared the results to the full spiking simulations. The techniques used in Ref. [36] should be applicable to the present model albeit with quenched variability. Furthermore, the resulting system will be a higher dimensional model primarily due to the time dependence of the synapses in our paper.

We studied the shapes of the PRFs of the EI network by computing the adjoint eigenfunctions for the linearized Fokker-Planck operator in order to see if there was any clear difference between them depending on the strength of synaptic connections and the mechanism underlying the gamma oscillations. In Figs. 3(a) and 3(b), Z_I are generally sinusoidal because the parameters are close to the Hopf bifurcation point and the dynamics becomes similar to the normal form of Hopf bifurcation [32]. We found the amplitude of PRF becomes smaller as the parameter moves away from the bifurcation point as shown in Figs. 4(b) and 4(e). The transition of amplitude of PRF is consistent with the normal form of Hopf bifurcation

[32]. In contrast, in Fig. 4(c), the amplitude of Z_E became larger. This is because the increase of p_{IE} causes an increase of the effect of the E population on the I population. Overall, we found that the PRFs were similar in shape independent of the mechanism of gamma generation with the excitatory response consistently weaker than the inhibitory.

We also found the amplitude of Z_E is quite different between the ING case and the PING case, as shown in Figs. 4(g) and 4(h), while the frequency of the oscillation and Z_I have smaller differences. This is because the contribution of the E population to the rhythmogenesis is largely different in the ING and PING cases. In the ING case, the driver for I cells is just bias current I_I, and excitatory cells are essentially disconnected to I cells. Therefore, the rhythm is insensitive to stimulation of the E cells and the amplitude of Z_E is zero. In the PING case, E cells are driving I cells, so the amplitude of Z_E is larger than that of ING. As these results show, the amplitude of Z_E reflects the inner structure of the neuronal population, in this case how strong the E cells are connected to I cells, which is difficult to measure directly in physiological experiments. Also, estimating Z_E makes it easier to distinguish whether the generation mechanism of the gamma oscillation is more ING-like or PING-like.

Curiously, for some combinations of parameters (cf. Fig. 5), the PRF is non-negative even close to the Hopf bifurcation. Non-negative PRFs are characteristic of type-I excitability and a saddle node on a circle bifurcation [38]. Further study of the FPE is needed to better understand why the PRF is non-negative near the bifurcation. We note that Akam *et al.* [9] (Fig. 5) computed the PRF for hippocampal gamma rhythms and found it to be quite similar to those shown in Fig. 3 of this paper.

In order to explore the consequences of differences between the PRFs of excitatory versus inhibitory populations, we also studied the locking regimes to periodic pulsatile stimuli to either the E or the I populations. We found that the locking region of the inhibitory population is wider than that of the excitatory population showing that stimulating the I population is better for entrainment of gamma-band frequencies. This result supports our assertion that the origin of the cell-type-specific response, which Cardin *et al.* found [33], comes from the difference of the entrainment ability to pulsatile stimuli. In addition, comparing ING and PING, we found that stimulating E cells in the PING oscillation had a wider locking region than was the case for ING-based oscillations. This result suggests such differences in the spiking population could lead to an efficient way to distinguish ING and PING in biological experiments. Also, we remark that we can roughly infer the entrainment ability to the pulsatile stimuli from just the amplitude of phase response function Z_X. In Fig. 4, the amplitude of Z_I was larger than that of Z_E, which implies that the I population has a wider locking region. This analysis shows that macroscopic phase response reduction, which is based on the macroscopic phase response function, provides a rigorous and efficient way to analyze the synchronization phenomena of gamma oscillations, even in large networks.

We finally note that using the PRFs that we have computed here, it will be possible to study the effects of coupling and synchronization across multiple regions in the brain. That is, we can apply weak-coupling theory and use this to study large-scale phase models of cortical networks in which the interactions are based on the rigorous reduction of noisy spiking networks. We remark that, since most long-range connections in cortical networks are excitatory, PING will be much better at communicating synchrony than will ING.

ACKNOWLEDGMENTS

We would like to thank Miles A Whittington for fruitful discussion about the generation mechanisms of gamma rhythm. This study was supported in part by Grant-in-Aid for JSPS Research Fellow Grant No. 16J04952 to A.A. K.K. was supported by JST PRESTO (JPMJPR14E2) and SCOPE (142103017). G.B.E. was supported by National Science Foundation DMS 1712922. In this work, we used the computer of the MEXT Joint Usage/Research Center "Center for Mathematical Modeling and Applications," Meiji University, Meiji Institute for Advanced Study of Mathematical Sciences (MIMS).

[1] C. M. Gray and W. Singer, Proc. Natl. Acad. Sci. USA **86**, 1698 (1989).
[2] L. Melloni, C. Molina, M. Pena, D. Torres, W. Singer, and E. Rodriguez, J. Neurosci. **27**, 2858 (2007).
[3] G. Buzsaki and X.-J. Wang, Annu. Rev. Neurosci. **35**, 203 (2012).
[4] M. Bartos, I. Vida, and P. Jonas, Nat. Rev. Neurosci. **8**, 45 (2007).
[5] A. Fisahn, F. G. Pike, E. H. Buhl, and O. Paulsen, Nature (London) **394**, 186 (1998).
[6] M. A. Whittington, R. D. Traub, and J. G. R. Jefferys, Nature **373**, 612 (1995).
[7] A. Fisahn, S. F. Heinemann, and C. J. McBain, J. Physiol. **562**, 199 (2005).
[8] E. O. Mann, J. M. Suckling, N. Hajos, S. A. Greenfield, and O. Paulsen, Neuron **45**, 105 (2005).
[9] T. Akam, I. Oren, L. Mantoan, E. Ferenczi, and D. M. Kullmann, Nat. Neurosci. **15**, 763 (2012).
[10] C. Börgers and N. Kopell, Neural Comput. **15**, 509 (2003).
[11] C. Börgers and N. J. Kopell, Neural Comput. **20**, 383 (2008).
[12] G. B. Ermentrout and D. H. Terman, *Mathematical Foundations of Neuroscience* (Springer Science and Business Media, New York, 2010), Vol. 35.
[13] N. Brunel and X.-J. Wang, J. Neurophysiol. **90**, 415 (2003).
[14] T. B. Luke, E. Barreto, and P. So, Neural Comput. **25**, 3207 (2013).
[15] C. R. Laing, Phys. Rev. E **90**, 010901 (2014).
[16] K. Kotani, I. Yamaguchi, L. Yoshida, Y. Jimbo, and G. B. Ermentrout, J R. Soc., Interface **11**, 20140058 (2014).
[17] C. Borgers, G. T. Franzesi, F. E. LeBeau, E. S. Boyden, and N. J. Kopell, PLoS Comput. Biol. **8**, e1002362 (2012).

[18] D. A. McCormick and J. R. Huguenard, J. Neurophysiol. **68**, 1384 (1992).
[19] M. Bartos, I. Vida, M. Frotscher, J. R. P. Geiger, and P. Jonas, J. Neurosci. **21**, 2687 (2001).
[20] A. Gupta, Y. Wang, and H. Markram, Science **287**, 273 (2000).
[21] C. Ly and G. B. Ermentrout, SIAM J. Appl. Dyn.l Syst. **9**, 113 (2010).
[22] H. Risken, *Fokker-Planck Equation* (Springer, New York, 1984), pp. 63–95.
[23] T. Kanamaru and M. Sekine, Neural Comput. **17**, 1315 (2005).
[24] W. Gerstner and W. M. Kistler, *Spiking Neuron Models: Single Neurons, Populations, Plasticity* (Cambridge University Press, Cambridge, UK, 2002).
[25] B. Ermentrout, *Simulating, Analyzing, and Animating Dynamical Systems: A Guide to XPPAUT for Researchers and Students* (SIAM, Philadelphia, 2002), Vol. 14.
[26] M. Strüber, J.-F. Sauer, P. Jonas, and M. Bartos, Nat. Commun. **8**, 758 (2017).
[27] Y. Kuramoto, *Chemical Oscillations, Waves, and Turbulence* (Springer, New York, 1984).
[28] Y. Kawamura, H. Nakao, K. Arai, H. Kori, and Y. Kuramoto, Phys. Rev. Lett. **101**, 024101 (2008).
[29] T. L. Williams and G. Bowtell, J. Comput. Neurosci. **4**, 47 (1997).
[30] B. Pfeuty, G. Mato, D. Golomb, and D. Hansel, J. Neurosci. **23**, 6280 (2003).
[31] T. J. Lewis and F. K. Skinner, *Phase Response Curves in Neuroscience* (Springer, New York, 2012), pp. 329–359.
[32] E. Brown, J. Moehlis, and P. Holmes, Neural Comput. **16**, 673 (2004).
[33] J. A. Cardin, M. Carlén, K. Meletis, U. Knoblich, F. Zhang, K. Deisseroth, L.-H. Tsai, and C. I. Moore, Nature (London) **459**, 663 (2009).
[34] J. Csicsvari, H. Hirase, A. Czurko, and G. Buzsaki, Neuron **21**, 179 (1998).
[35] E. Montbrió, D. Pazó, and A. Roxin, Phys. Rev. X **5**, 021028 (2015).
[36] G. Dumont, G. B. Ermentrout, and B. Gutkin, Phys. Rev. E **96**, 042311 (2017).
[37] E. Ott and T. M. Antonsen, Chaos **18**, 037113 (2008).
[38] B. Ermentrout, Neural Comput. **8**, 979 (1996).